Computational Materials Science 209 (2022) 111368

Contents lists available at ScienceDirect

Computational Materials Science

journal homepage: www.elsevier.com/locate/commatsci

Tensile characteristics of boron nanotubes by using reactive molecular dynamics simulations

Erdem Caliskan, Mesut Kirca *

Department of Mechanical Engineering, Istanbul Technical University, 34437 Istanbul, Turkey

ARTICLE INFO

Keywords:
Boron Nanotubes
Molecular Dynamics
Mechanical Properties

ABSTRACT

In this study, the mechanical behavior of BNTs with distinct morphologies subjected to tensile loading is investigated through reactive molecular dynamics simulations. For this purpose, atomistic models of eight different BNT morphologies with zigzag and armchair configurations are generated to be utilized in tensile testing. Furthermore, a reactive force field, namely ReaxFF, allowing continuous bond formation/breaking, is employed in MD simulations to conduct more realistic tensile simulations. Simulation results indicate that ReaxFF potential can represent key structural properties of BNTs, such as surface buckling and elliptic cross-section. Furthermore, it is demonstrated that Young's modulus and tensile strength of BNT structures highly depend on the vacancy ratio. In this regard, empirical formulae for Young's moduli and tensile strength of BNTs with non-zero vacancy ratios are proposed based on the BNT structure with zero vacancies (i.e., 2-pmmn). According to the overall results, it can be underlined that BNTs, which have comparable mechanical properties with carbon nanotubes, can be considered as an ideal analog of carbon nanotubes in diverse applications, including nanocomposites and nanoelectromechanical systems.

1. Introduction

The discovery of CNTs [1] and subsequently the synthesis of graphene [2] sparked a great doping effect for the subsequent research studies on low-dimensional materials. In addition to experimental studies trying to synthesize new low-dimensional nanomaterials, many researchers also presented theoretical studies with the aim of exploiting alternative materials [3]. In recent years, new two-dimensional nanomaterials, including silicene [4,5], germanene [6,7], and borophene [8,9], can be considered as the counterparts of graphene with the base elements of silicon, germanium, and boron, respectively, have been successfully synthesized. Owing to their extraordinary mechanical, electrical, and chemical properties, these low-dimensional materials attract significant attention from the scientific community.

Among these recently developed mono-layered nanomaterials, borophene presents remarkable properties due to the chemical and structural complexity of the fascinating element boron. Boron, the fifth element in the periodic table, is the lightest elemental substance that can form interatomic covalent bonds possessing multiple bonding states, which in turn provides formations of a variety of allotropes with diverse physical and chemical properties [10–12]. In low dimensional materials science, the synthesis of two-dimensional boron films, namely borophene, can be considered as crucial progress [3,8,9]. Similar to the carbon allotropes such as graphene, CNTs, and fullerenes, boron allotropes, including borophene and boron nanotubes (BNTs), gather significant attention in the scientific community due to their notable properties such as low density, high mechanical strength, and high melting point [13]. Among different allotropic forms of boron, BNTs with structural stability are firstly proposed by Boustani and A. Quandt in 1997 [14]. In their computational study, they predicted structural and electronic properties of BNTs and boron sheets using ab initio methods and concluded that the boron atoms could form several types of allotropic structures as well as boron nanotubes. Following the computational study presenting the existence of thermodynamically feasible BNT structures in 1997, Ciuparu et al. [15] successfully synthesized pure BNT structure on Mg-MCM-41 catalyst for the first time in 2004. Since then, there have been several other studies concerning the synthesis of BNTs. For instance, Liu et al. [16] accomplished to fabricate single-walled BNTs with diameters between around 10 to 40 nm using a thermal evaporation method and studied their electric transport and field

* Corresponding author at: Address: Department of Mechanical Engineering, Istanbul Technical University, Inonu Cad. No: 65 34437, Gumussuyu, Istanbul, Turkey.
E-mail address: kircam@itu.edu.tr (M. Kirca).

https://doi.org/10.1016/j.commatsci.2022.111368
Received 14 December 2021; Received in revised form 7 March 2022; Accepted 16 March 2022
Available online 23 March 2022

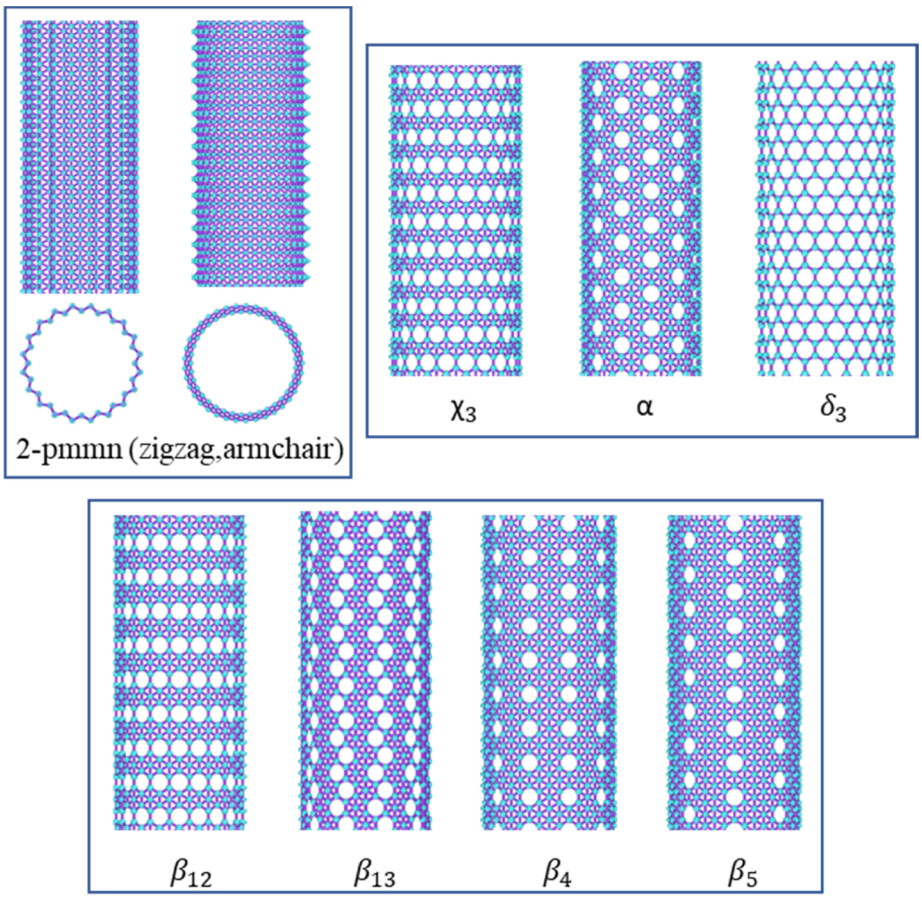

Fig. 1. BNTs that has been studied in this work. Structures with vacancies are in zigzag direction.

emission properties, showing that individual BNTs can sustain high current densities. Furthermore, Liu and Iqbal [17] managed to synthesize single-walled BNTs with a diameter of around 20 nm and double-walled BNTs with a diameter of around 10 nm.

CNTs, which have been successfully synthesized approximately one decade before graphene and regarded as a substantial driver for the scientific research on the nanomaterials, can be either metallic, semiconductor, or insulator depending on their radii and chirality [18,19]. This generally suggests a weak control over the electronic properties of CNTs in specific applications [20]. Even though some reports claiming α-boron nanotubes (α-BNTs) with diameters less than 1.7 nm [21,22] or 2 nm [23] might show semiconducting behavior due to the band opening in Fermi level through curvature-induced out-of-plane buckling of certain atoms; subsequent calculations based on second-order Møller–Plesset perturbation theory [24] and dispersion-corrected density-functional calculations [25] and experimental studies [16] showed that the surface buckling might be an artifact of standard DFT. Thus, researchers concluded that, without surface buckling, all α-BNTs are indeed metallic [26]. In the same study, Bezugly et al. [27] conducted density functional studies on BNTs rolled from α-, 2-pmmn (buckled triangular), and distorted hexagonal sheet, and reported that these BNTs are metallic, irrespective of their lattice types, radii, and chirality, and, highly conductive. In a recent study, Wu et al. [28] have studied electron transport through BNTs rolled from β_{12}-borophene conducting DFT calculations, and showed that the BNTs exhibit metallic behavior regardless of chirality and tube diameters even though the atoms in the hexagonal centers are buckled. The fully metallic behavior of BNTs renders them extremely attractive in the design of novel electronic nanodevices, such as field-effect transistors, light-emitting diodes, field emission displays [13]. In these applications, mechanical properties have a significant role since the mechanical strain (tension or compression) is usually employed to modify the electronic properties of the BNTs [29]. Therefore, mechanical properties of the BNTs with different lattice structures such as tensile strength and elastic Young's modulus hold prominent importance.

It is well known that in addition to their inherent uncertainties, experimental methods are extremely complex and expensive to investigate the properties of nanostructured materials, which promotes numerical simulation techniques as promising alternatives [30]. In this regard, for the purpose of examining the mechanical, electrical, and chemical properties of BNTs, there exist several numerical studies employing density functional theory (DFT) and molecular structural mechanics (MSM) techniques. For example, by performing DFT calculations, Tang and Ismail-Beigi [31] demonstrated that new boron sheets with mixed triangular and hexagonal lattices might exist. They also revealed that those boron sheets with non-zero hexagonal hole densities, i.e., η (ratio of the number of hexagon holes to the number of atoms in the original triangular sheet), are stable and can be the precursors of BNTs. Moreover, in a later work [23], they studied structural, energetic, and electronic properties of single- and double-layered boron sheets as well as single- and double-walled boron nanotubes by using the same method. Along the same line, Sebetci et al. [20] studied the structural, energetic, and electronic properties of the double-walled 2-pmmn BNTs ($\eta = 0$) by using DFT calculations and proved that the structures have metallic behavior. In a different study, Kunstmann and Quandt [32,33] explored the geometry, energetics, and basic chemical properties of 2-pmmn BNTs ($\eta = 0$) by conducting ab initio calculations and confirmed that zigzag BNTs with small diameters tend to have puckered surfaces. In another work, Kunstmann et al. [33] showed that the single-walled α-, 2-pmmn (buckled triangular), and distorted hexagonal BNTs were thermally stable at synthesis temperature using DFT-based molecular dynamics. Regarding mechanical behavior, Evans et al. [34]

studied mechanical properties of 2-pmmn BNTs using local density approximation (LDA) to density functional theory and calculated Young's moduli as 490 and 290 N/m in zigzag and armchair directions, respectively. In a later work, Kochaev [35] investigated the elastic properties of BNTs with diameters between around 0.2 to 2 nm rolled from 2-pmmn boron sheet (η = 0) by DFT calculations by presenting that Young's moduli of BNTs are around 1680 and 825 N/m for zigzag and armchair directions respectively. Researchers didn't comment on the difference of the values with the previous work. Besides that, not very long ago, Zhang and Zhou [36] studied the buckling characteristics of α-BNTs and χ-BNTs under axial compression using DFT-based MSM simulations and elastic continuum shell models. They noted that buckling mode transitions from shell buckling into column buckling could be observed with the increase in the aspect ratio. Recently, Aziz et al.[37] studied mechanical properties of 2-pmmn boron nanotubes using non-reactive molecular dynamics. They have used Stillinger-Weber (SW) potential field [38] to model the interactions between atoms, yet SW and some other potential fields are incapable of modeling BNTs for several reasons. The first one is that, even though it can successfully model the non-linear components, it is only applicable to the triangular phase of the borophene. Secondly, this three-body potential does not work for BNTs at room temperature, based on our preliminary simulations. Thus, they only simulated BNTs up to 100 K temperature.

Considering the studies in literature examining the physical behavior of BNTs, most of the theoretical studies regarding the boron nanotubes are based on the first-principles density functional theory (DFT) calculations. Although quantum mechanics-based DFT calculations provide fairly more accurate results compared to higher-level techniques such as classical molecular dynamics (MD), it is practically limited to the structures consisting of up to approximately 1000 atoms due to huge computational expense [38]. For this reason, classical MD simulations, which are widely utilized to explore the physical and chemical properties of nanostructured materials, can be used to investigate much larger systems as an alternative approach. In the present study, boron nanotubes are investigated using reactive molecular dynamics simulations. Although reactive molecular dynamics has been extensively practiced for some borophene monolayers [30,39–43], to the best of our knowledge, it has not been used to simulate BNTs yet. With this motivation, in this study, the mechanical characteristics of BNTs constructed from 10 different borophene allotropes are investigated by employing reactive interatomic potential. Each BNT sample with different hexagonal hole densities is subjected to tensile loading at different temperatures. Mechanical characteristics, including Young's modulus and ultimate strengths, are evaluated and employed to make comparisons between different BNT types. Some empirical formulae which are parametrized with vacancy ratio are developed to predict the tensile characteristics of BNTs. Furthermore, effects of morphological variations such as stable bond formation and cross-sectional alterations during tensile straining on the mechanical response are evaluated to explain the distinctive observations on the stress-strain curves.

2. Methodology

In the present study, classical MD simulations are performed to investigate the mechanical properties of BNTs composed of different borophene allotropes shown in Fig. 1. Figs. in this article are illustrated using the OVITO tool [44]. The interactions between the boron atoms are modeled using a reactive force field known as ReaxFF permitting continuous bond formation/breaking and developed by Adri van Duin et al. [45]. ReaxFF$_{CBN}$ parameterization has been developed by Pai et al. [46] for the simulation of liquid carbon-boron-nitrogen materials provides remarkably accurate results with respect to the first principles predictions available in the literature [30,41]. In literature, there are some other potentials that are used to examine boron-based nanostructures. For instance, Zhou et al. has developed a non-reactive force field (Stillinger-Weber potential) [38] which is only capable of representing force field in 2-pmmn (η = 0) quasi-planar structure. In this regard, there are no force fields to represent all of the allotropes of borophene sheets other than ReaxFF within the knowledge of the authors.

The most important terms of the total energy of an atomic system close to equilibrium can be given as follows [47]:

$$E_{sys} = E_{bond} + E_{angle} + E_{torsion} + E_{Vd\ \ Waals} + E_{Coulomb} \tag{1}$$

$$E_{\text{bond}} = k_b(r - r_0)^2 \tag{2}$$

$$E_{angle} = k_v(\varphi - \varphi_0)^2 \tag{3}$$

$$E_{\text{torsion}} = V_2(1 - \cos(2\omega)) + V_3(1 - \cos(3\omega)) \tag{4}$$

$$E_{\text{VdWaals}} = D_{ij}\left\{ e^{\alpha_{ij}\left(1-\frac{r_{ij}}{r_{\text{VdW}}}\right)} - 2e^{\frac{1}{2}\alpha_{ij}\left(1-\frac{r_{ij}}{r_{\text{VdW}}}\right)} \right\} \tag{5}$$

$$E_{Coulomb} = C\frac{q_i q_j}{r_{ij}} \tag{6}$$

where E_{sys}, E_{bond}, E_{angle}, $E_{torsion}$, $E_{VdWaals}$, and $E_{Coulomb}$ are the energy of the system, bond, angle, torsion, and non-bonded van der Walls and Coulombic energies, respectively. ReaxFF potential includes additional energy types such as double-bond valence angle penalty, valence angle conjugation energy, hydrogen bond energy, etc. Some of these terms can be neglected based on the dynamics of the system [48].

In this study, some computer codes are developed to generate the initial configuration of the borophene structures and then to transform them into BNTs. BNT allotropes with different numbers of missing atoms or vacancies from the original triangular sheet (η) studied in this work are given in Fig. 1. Lattice parameters are taken as 1.614, 2.866, and 0.911 Å in *a, b,* and *h* directions for quasi-planar structures [49] and 2.926 and 5.608 Å for planar structures [50], respectively. The diameters and lengths of the structures are given in Table S1. MD simulations are conducted using the Large-scale Atomic/Molecular massively Parallel Simulator (LAMMPS), which is an open-source code [51], with velocity Verlet time-integration algorithm. We used ReaxFF and ReaxC-OMP packages, implemented by Aktulga et al. [52,53]. The periodic boundary condition is applied in the longitudinal direction for the avoidance of the boundary effects. For boron nanotubes, 50 Å vacuum is defined for the lateral (i.e., radial) direction. The specimens are relaxed to zero stress state with NPT ensemble using the Nosé-Hoover barostat and thermostat method for 1 ps. Uniaxial tensile tests are carried out by applying a constant engineering strain rate which is selected as 1×10^9 (1/s). The size of the simulation box along the direction perpendicular to the loading (i.e., longitudinal) direction is controlled with the assumption of NPT ensemble to achieve zero stress condition along the edge lateral to the loading direction in order to guarantee uniaxial stress conditions.

Stress tensor is calculated by using the virial stress theorem as given in Eq. (7) [30]

$$\sigma = \frac{1}{V}\sum_{i\in V}\left[-m^{(i)}v^{(i)} \otimes v^{(i)} + \frac{1}{2}\sum_{i\neq j} r^{(ij)} \otimes f^{(ij)} \right] \tag{7}$$

where $m^{(i)}$, $v^{(i)}$, $r^{(i)}$, $r^{(ij)}$, $f^{(ij)}$, and V are the mass and velocity vector of the atom, the position of the atom *i*, the distance vector between the atoms *i* and *j*, the interatomic force applied on atom *a* by atom *b*, and the volume of the structure, respectively. In recent experimental studies, inconsistent numerical values, including 2.9, 3, 4.2, and 5 Å, are reported for the thickness of the boron films [8,54–56]. Due to this ambiguity, we submit Young's modulus and stress values in the form of $E \bullet t$ and $\sigma \bullet t$, respectively, where t is the thickness.

The engineering strain is calculated as:

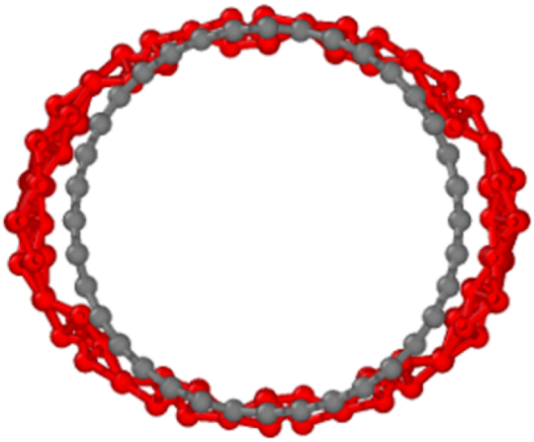

Fig. 2. Initial (gray) and final (red) structures of BNTs during energy minimization. α-BNT is given as an example. (For interpretation of the references to colour in this figure legend, the reader is referred to the web version of this article.)

$$\varepsilon^{t} = \frac{L_x^t - L_x^0}{L_x^0} \tag{8}$$

where ε^t and $L_x{}^t$ is the engineering strain and length along longitudinal (i.e. x) direction at the instant respectively and $L_x{}^0$ is the initial length along $\times$ direction.

3. Results and discussion

Each BNT configuration minimized through conjugate gradient method with the utilization of ReaxFF potential field is shown to be thermally stable under an isothermal-isobaric ensemble. Simulation results indicate that the lattice parameters change, which has been reported previously for the borophene structure by Mortazavi et al. [40]. They noted that the results are not affected by this inaccuracy of the potential field. We observed a similar situation regarding BNTs. The simulation box increases in size by 10% and 20% in axial and preferred radial directions, respectively. The elliptic cross-section is a structural property of BNTs due to the bands in the Fermi level. The details of this property are explained by Kunstmann et al. [26]. In their article, using DFT simulations, it is demonstrated that energetically most favorable BNT structures have elliptical cross-sections. Our results agree with DFT simulations, which is an indicator of the capability of ReaxFF for the mechanical simulation of BNTs. The shape change of the cross-section is given as an example for α-BNT structure in Fig. 2.

According to the simulation results, another common structural property of BNTs originated from planar borophenes is the surface buckling of atoms located at the hexagonal center, which is also reported by Tang and Ismail-Beigi [23] in their first-principles study. As a result of surface buckling, the radial locations of the atoms are altered even at 1 K temperature, as depicted in Fig. 3. Therefore, it is noteworthy that the ReaxFF force field can also represent the surface buckling property of BNTs. These aforementioned structural similarities with DFT calculations imply that the ReaxFF force field is capable of representing key structural features of BNTs.

Stress-strain curves of twenty different BNT configurations at room temperature are given in Fig. 4. In order to provide a quantitative examination, numerical values for several mechanical characteristics of all configurations, including ultimate tensile stress, strain, and Young's moduli calculated at three different temperatures (i.e., 1 K, 300 K, and 600 K) are also given in Table S2. Moreover, in order to make comparisons easy, stress-strain curves of all specimens with zigzag and armchair configurations at room temperature (i.e., 300 K) are provided as a supplementary document in Figs. S2 and S3, respectively. Amongst all BNT structures, it is seen that the zigzag configuration of the 2-pmmn structure has much higher stiffness and ultimate tensile strength compared to the other BNTs, while its ultimate strain is much less than most of the other structures due to high brittleness. Furthermore, it can also be noted that depending on the configuration, significant distinctions between the armchair and zigzag directions are observed for some BNTs, including 2-pmmn, δ_3, and χ_3. The main reason for this distinction is the configurational dissimilarities of bond and/or hole arrangements along with different directions. Considering the stress-strain curves of zigzag and armchair directions for each BNT type, the β_{13} structure has the highest isotropy for the armchair and zigzag directions.

The potential energy distribution is the main driving force for these differences. If the potential energy is evenly distributed, the structure can preserve the homogeneous shape, which results in more brittle behavior during the tensile. For example, the 2-pmmn zigzag cross-section, given in Fig. 5a, represents the most homogeneous potential energy distribution. This structure is highly brittle and has the highest Young's moduli, thus the stiffest structure. Another example is the β_{12} zigzag structure, given in Fig. 5b. In this one, the potential energy is not homogeneous as the 2-pmmn, yet the distribution is small enough that it can form a semi-circular shape. However, some structures, such as β_{13}, given in Fig. 5c, have a high potential energy gradient; thus, the cross-section has a hollow shape. This type of cross-section results in a more ductile tensile behavior. Finally, the last type is the rectangle-like cross-section like β_5, given in Fig. 5d. These structures tend to behave in between brittle and ductile fractures. They can still carry some load after ultimate tensile stress, but not as much as the ductile behaving structures like β_{13}.

The cross-section evolves to different kinds of shapes due to the Poisson effect, which is later explored in detail in the following sections. The main impact of this effect is the bond formation due to contraction. The direction and the stability and/or instability of these forming/deforming bonds determine the mechanical response of the material.

The 2-pmmn zigzag configuration has the highest tensile strength compared to all other structures examined in this study (Fig. 4). The major factor yielding the highest strength is originated from the bonding arrangement of the 2-pmmn zigzag structure. According to that, the bonds oriented along the direction of loading constitute continuous beam-like support throughout the nanotube, which increases both the stiffness and the strength of the 2-pmmn zigzag structure.

Fig. 6 illustrates the tensile stress-strain curves of zigzag and

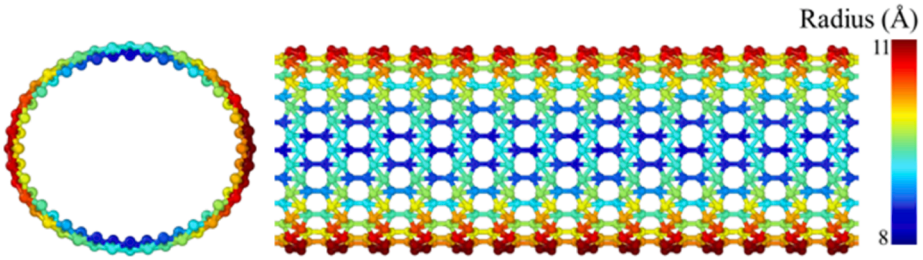

Fig. 3. Radius distribution through BNT structure after thermalization for 0.1 ps at 1 K. χ_3-BNT zigzag is given as an example.

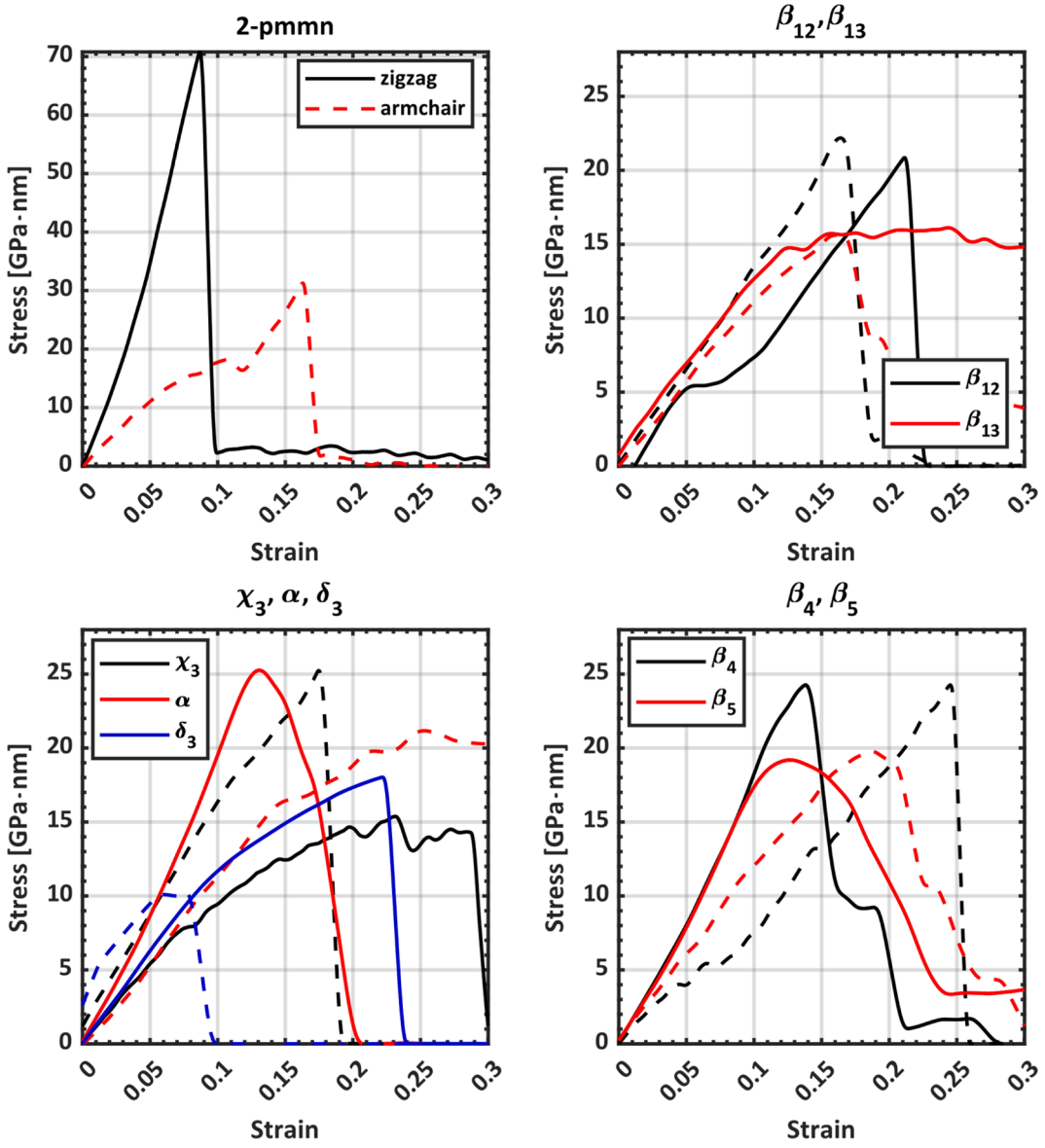

Fig. 4. Stress–strain comparison for BNTs at 300 K, straight lines are zigzag, and dashed lines are armchair configurations.

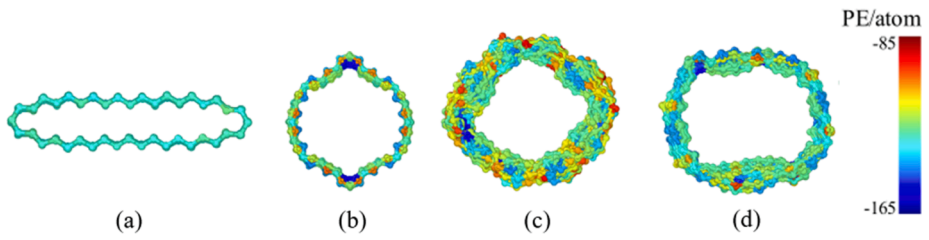

Fig. 5. Cross-section of the structures after thermalisation at 300 K. (a) 2-pmmn, (b) β_{12}, (c) β_{13}, (d) β_5 zigzag configurations.

armchair type 2-pmmn structure at different temperatures. According to that, tensile strengths and bond-breaking strains of both zigzag and armchair 2-pmmn nanotubes tend to decrease as the temperature increases, while no significant change in Young's modulus is observed. The decrease in the strength and ultimate strain values with increasing temperature can be attributed to the increased thermal energy stimulating the disintegration of atoms.

The stress-strain curve of the 2-pmmn armchair structure (see Fig. 6b) has two different linear regimes, which is similar to the planar borophene structure [40]. These two distinct regimes separated with an intermediate softening regime are due to the process of aligning out-of-plane atoms with the in-plane atoms as a result of tensile straining. The non-homogeneous cross-section of the structure turns into a homogeneous cross-section with a complex wavelike circle with all atoms in the tensile direction, as depicted in Fig. 7b.

The cross-section of the structure is not uniform after the thermalization. Potential energy per atom is also not homogeneous due to the shape of the cross-section. This rectangle-like shape has different bond

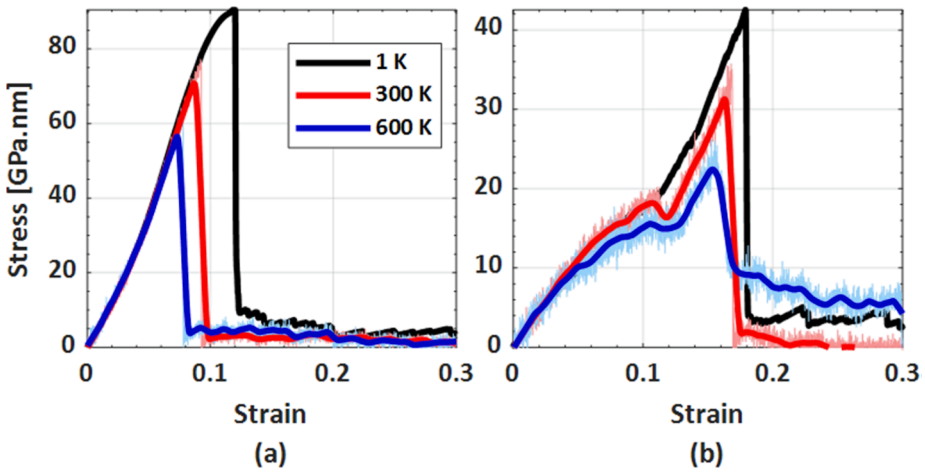

Fig. 6. Stress–strain curves of 2-pmmn-BNT for (a) zigzag and (b) armchair configurations.

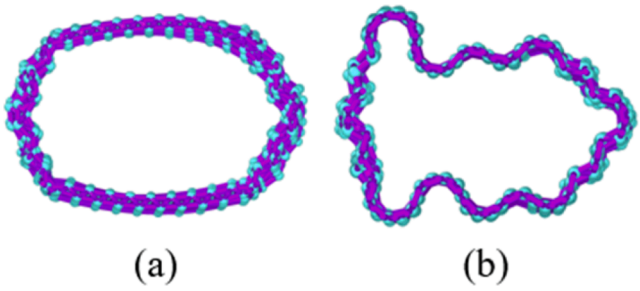

Fig. 7. Cross-section of 2-pmmn armchair configuration at 1 K.

energies across the cross-section owing to their distinct curvatures. Thus, high local potential energy gradients reduce the stability of the 2-pmmn armchair BNT structure and create a non-linear stress-strain curve. High potential energy gradient causes defect formation, which in turn propagates to failure. In addition, the potential energy gradient increases with the temperature, which consequently increases the strain gradient.

In contrast to armchair structure, a single regime up to the rupture point is observed for the zigzag configuration of the 2-pmmn structure. Further elaboration of the failure mechanism indicates that the tensile load is primarily supported by the bonds parallel to the loading direction. The linear regime up to the ultimate strain state primarily corresponds to the elongation of these axial bonds. For all temperature values, the axial bonds inherently along the loading direction elongate uniformly without any local bond breakages. For the specimen tested at 1 K, axial bond elongations do not cease up to the strain state of 11.47%, at which all the axial bonds that sustain the tensile load break suddenly, as depicted in Fig. 8. Following the breakage of the axial bonds, the rupture of the nanotube is observed through a shear band (see Fig. 9) inclined to the tensile direction. Owing to the thermal energy of the atoms, the failure of the nanotubes at room temperature (i.e., 300 K) or at higher temperature (i.e., 600 K) occurs before the breakage of the axial bonds, as the shear band formation is induced by thermal vibrations.

Excluding the out-of-plane structure (i.e., 2-pmmn), all the other planar BNT structures can be considered as nanoporous structures due to having a non-zero vacancy ratio. It is very well known that the effective mechanical properties of the cellular solids highly depend on the relative density, which is defined as the ratio of the densities of the cellular solid and bulk solid. Considering the analogy between the relative density and the vacancy ratio, it can be noted that Young's moduli and the ultimate tensile strength of porous BNT structures tend to decrease with increasing vacancy ratio (see Fig. 10). Moreover, it is also noticed that vacancy ratio is not the only parameter affecting the mechanical behavior of BNTs.

Considering the vacancy-dependent behavior similar to the nanoporous materials, the following power law between the vacancy ratio and ultimate tensile strengths of the structures can be derived based on the numerical results:

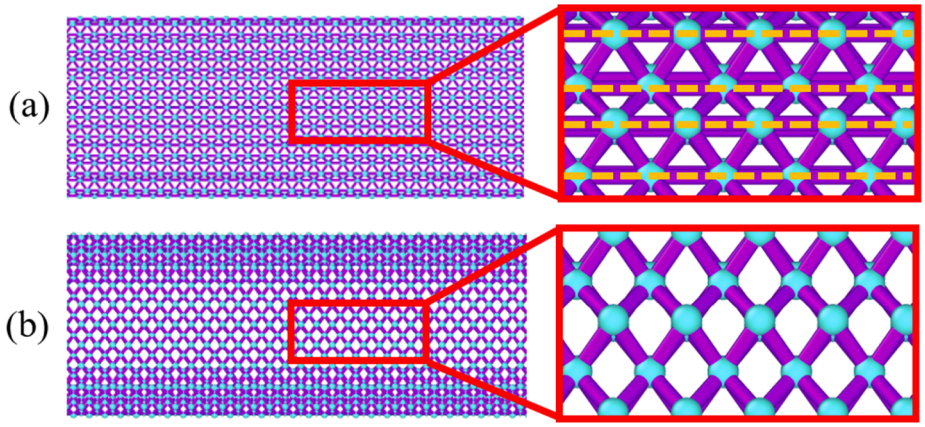

Fig. 8. Bond breakage for 2-pmmn zigzag structure. Bonding scheme at (a) 11.12% and (b) 11.47% strain states. Yellow dashed lines depict the axial bonds. (For interpretation of the references to colour in this figure legend, the reader is referred to the web version of this article.)

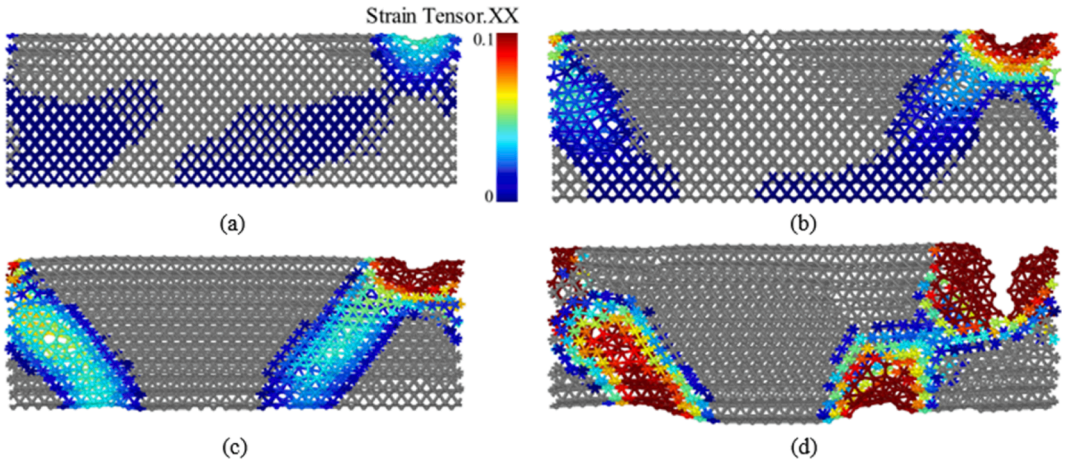

Fig. 9. Crack growth for 2-pmmn zigzag structure. Defect forms at 12.03% elongation (a) and rapidly grows at a 45-degree angle. Snapshots are at (b) 12.04%, (c) 12.05%, and (d) 12.15% elongations, respectively. Atoms and bonds are colored according to their respective strain level.

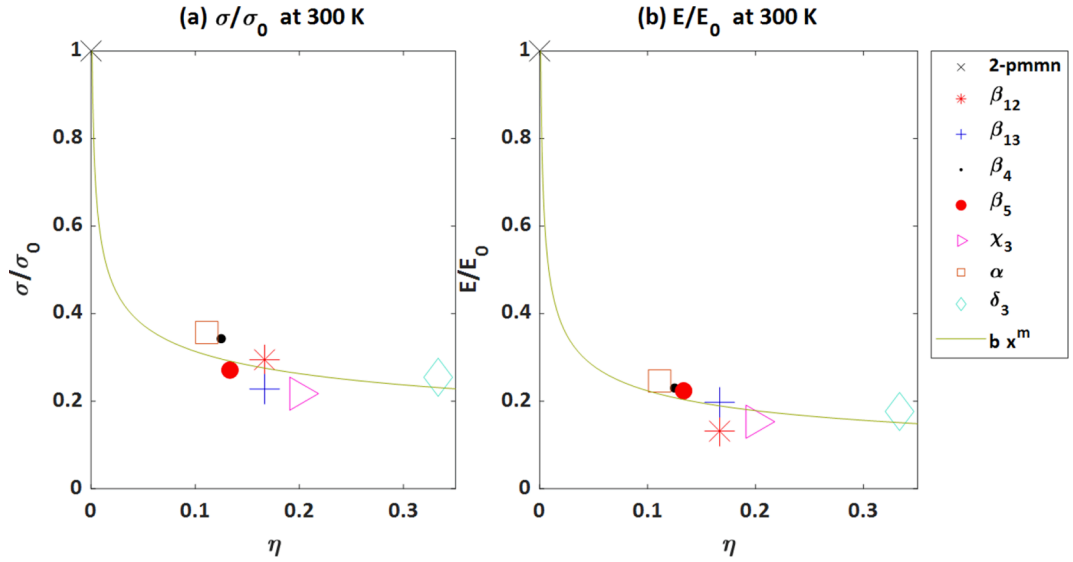

Fig. 10. Change of (a) ultimate tensile strength and (b) Young's moduli of structures with respect to vacancy ratio, η, at room temperature.

$$\frac{\sigma^{ut}}{\sigma_0^{ut}} = C{\cdot}\eta^{m} \tag{9}$$

where σ^{ut} and $\sigma_0{}^{ut}$ are the ultimate tensile strengths of the porous and non-porous BNT (i.e., 2-pmmn), respectively. C and m are the empirical constants of the power function, and η is the vacancy ratio. Using the results given in Fig. 10, C and m are found as 0.1748 and −0.2541, respectively. A similar relationship is developed for Young's modulus variation by Eq. (10):

$$\frac{E}{E_0} = D{\cdot}\eta^{n} \tag{10}$$

where E and E_0 are Young's moduli of the porous and non-porous BNT (i.e., 2-pmmn), respectively. D and n are the empirical constants of the power function. Using the results given in Fig. 10, D and n are found as 0.1056 and −0.3262, respectively. These power-law relationships for the ultimate tensile strength and Young's moduli can be updated by using the results from a wider range of vacancy ratios.

In order to examine the interesting mechanical characteristics of β group BNT configurations (i.e., β_{12} and β_{13}), tensile stress-strain curves at different temperatures are provided in Fig. 11. Stress-strain curves for β_4-zigzag and β_4-armchair structures are given in the supplementary document in Fig. S1. According to the curves, it is easily noticed that mechanical responses of the β type BNTs are significantly different, which clearly indicates the importance of the spatial arrangement of the atoms. Despite the equivalency of the vacancy ratios, β_{13} type BNT has much higher ductility compared to β_{12} structure. Simulation results also demonstrate that the β_4-BNT zigzag has the highest tensile strength and Young's modulus among the β structures. As another observation, it can be noted that armchair configurations generally have higher fracture strain compared to zigzag configurations owing to their bond angles. Unlike the bonds in the zigzag structure, the bonds in armchair structures are not oriented along the loading direction. Therefore, tensile deformation proceeds with the inclination of the bonds instead of elongation. As a result, they have higher ductility, which is in accordance with the DFT results reported by Kochaev [35].

In β structures, the spatial distribution of atomic potential energies is highly inhomogeneous at the unit cell level due to the diversity of the bond orders of the atoms. Yet, as depicted in Fig. 12, the potential energies of the atoms across the longitudinal axis of the nanotube repeat the same pattern within the unit cells. Thus, some β (e.g., β_4 and β_5) and other BNTs having similar PE distributions that are χ_3 and α, are more robust to preserve their circular cross-sections.

At 1 K temperature, the stress-strain curve of the β_{12}-BNT armchair

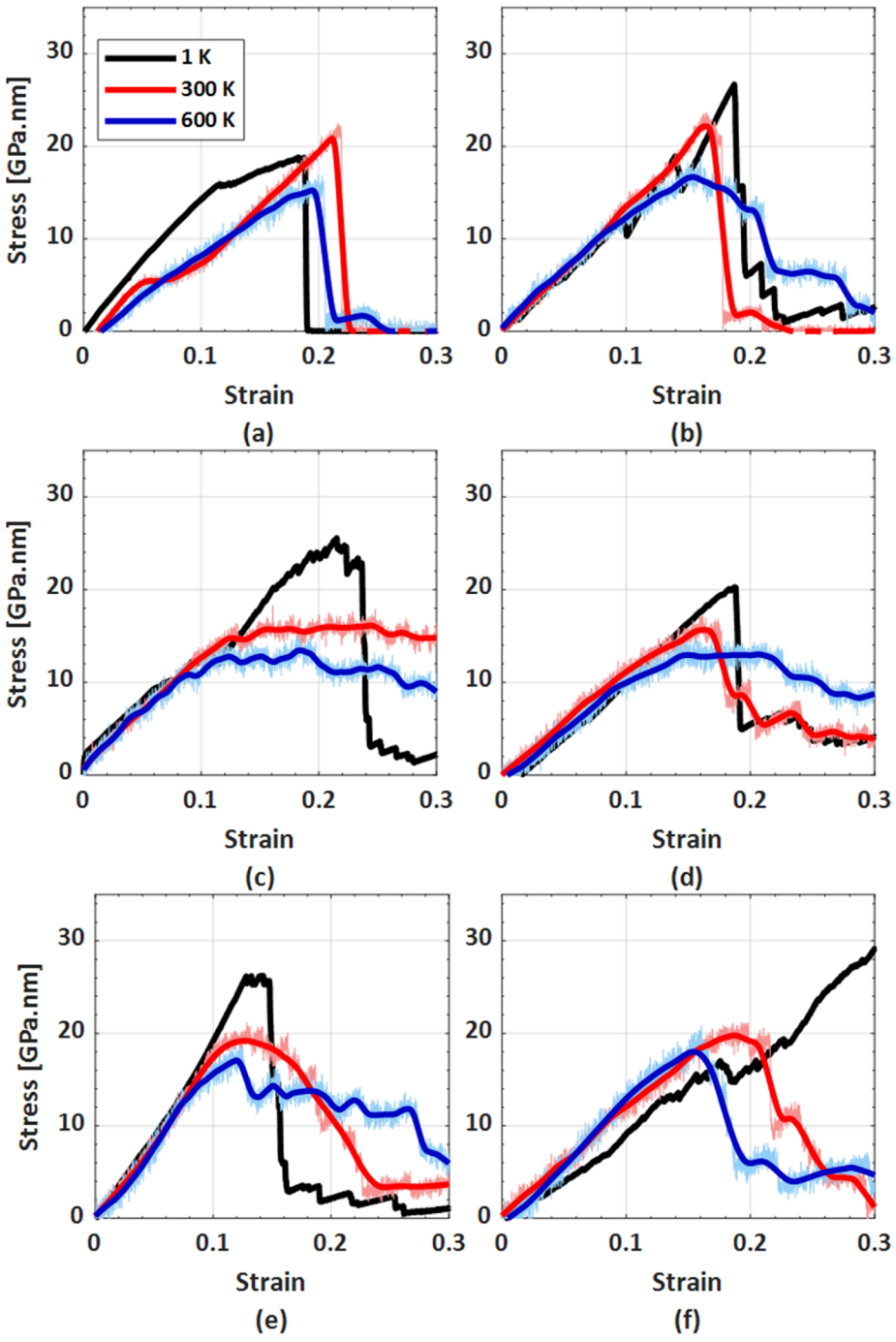

Fig. 11. Stress–strain curves of (a) β_{12}-zigzag, (b) β_{12}-armchair, (c) β_{13}-zigzag, (d) β_{13}-armchair, (e) β_5-zigzag and (f) β_5-armchair.

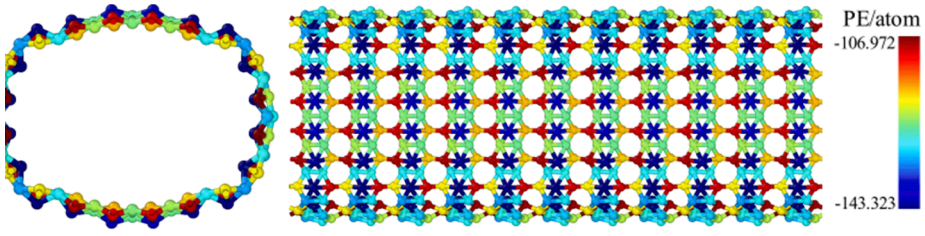

Fig. 12. Potential energy distribution per atom for the β_{12}-BNT zigzag at 1 K.

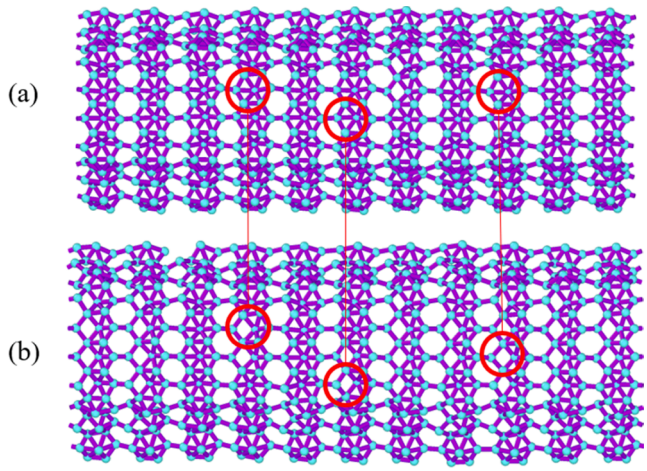

Fig. 13. State of bonds for zigzag β_{12}-BNT at (a) 4% elongation and (b) at 7% elongation at 300 K.

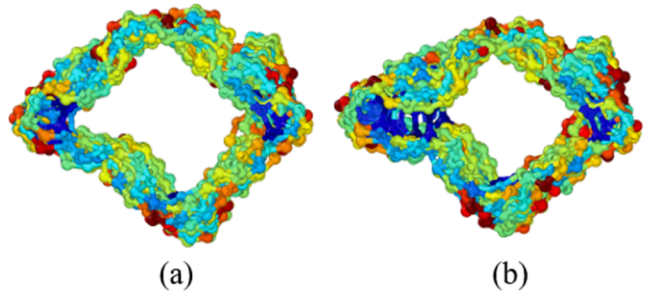

Fig. 14. Cross-section of zigzag β_{13}-BNT during tensile at 300 K. (a) at 12% elongation and (b) at 14% elongation.

structure possesses high instabilities around approximately 12% strain state owing to instantaneous formation and breakage of the bonds. On the other hand, at the same temperature, the zigzag configuration does not have any steep fluctuations due to bond breakage and formations. Furthermore, at 300 K, approximately 100 bonds (i.e., 4% of the bonds) break in the zigzag structure at around 6–8% strain state, generating a plateau regime that is followed by a stiffer response after the breakage process ends. The bond breakage and contraction for the β_{12} zigzag BNT are given in Fig. 13. The circled areas in Fig. 13a and b show the breaking bonds.

However, a similar stable and uniform bond formation process assisted by lateral contraction is not detected at 600 K due to high thermal energy, which in turn yields a lower strength. The bond formation at 300 K creates a unique situation for the zigzag β_{12}-BNT structures, making them the only structure with an increased strength compared to 1 K temperature.

Similarly, we also observe stable bond formation in zigzag β_{13}-BNT at 300 K. However, in zigzag β_{13}-BNT, bond formations start around 12% strain state and continue until fracture. Thus, stress levels do not increase while the straining proceeds. Since the bonds are in the radial direction, they don't harden the material, yet they cause the nanotube to collapse, as shown in Fig. 14.

On the other hand, as inferred from the stress-strain curves having no hardening regimes (see Fig. 15), nearly no bond formations are observed during the tensile straining of some BNT structures such as α-BNTs which are regarded as the most stable BNT structure by previous a study [27]. For instance, the increase in the bond numbers in tensile straining is approximately 1% and 2% for zigzag and armchair configurations of α-BNTs. Owing to their significant structural stability, α-BNTs, which are one of the BNTs with the highest tensile strength in the zigzag direction, are very ductile along the armchair direction. It should also be noted here that the ductility of the α-BNT increases with the temperature while their ultimate tensile strength decreases.

χ-BNT (Fig. 16) has the highest ductility among other BNTs in the zigzag direction. Interestingly, ductility is lower along the armchair direction, unlike other BNTs. This observation can be attributed to the different arrangements of the hexagonal holes along with the zigzag and armchair directions. According to that, as the holes in the armchair direction align with the longitudinal axis of the nanotube in the armchair direction, the response of the BNT is much stiffer owing to the fact that the thin ribbons between the longitudinal rows of the holes act as rod-like structural units. Increased stiffness results in earlier fracture, causing lower ductility for armchair direction.

δ_3-BNT, structured with a graphene-like hexagonal lattice, is shown to have the highest thermal stability. The structure has almost no thermal noise in the stress-strain, as can be seen in Fig. 17. However, the structure is found to be unstable in the armchair configuration for the preferred diameter used in tensile simulations. Structural instability is also observed by Kunstmann et al. [26] in their DFT study for the distorted hexagonal BNT with approximately the same diameter. They also report that the 2-pmmn structure is unstable while we observe the opposite case for the BNT with a larger diameter. Therefore, it can be inferred that the hexagonal structure might possess thermal stability with a larger diameter, in which case the potential energy gradient decreases with a decrease in curvature.

Tensile characteristics of the BNT specimens (i.e., 2-pmmn, β_4, β_{12}, and χ_3) are also examined for different strain rate values, which are 10^8,

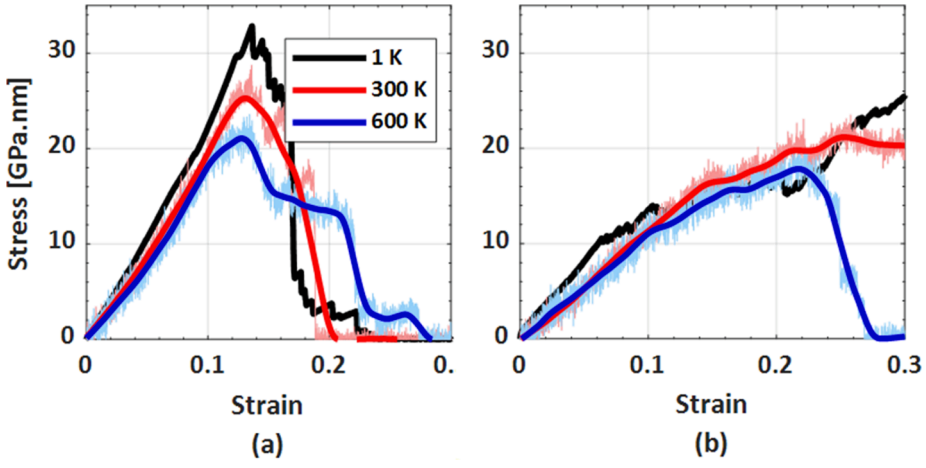

Fig. 15. Stress–strain curves of α-BNT, (a) zigzag, (b) armchair.

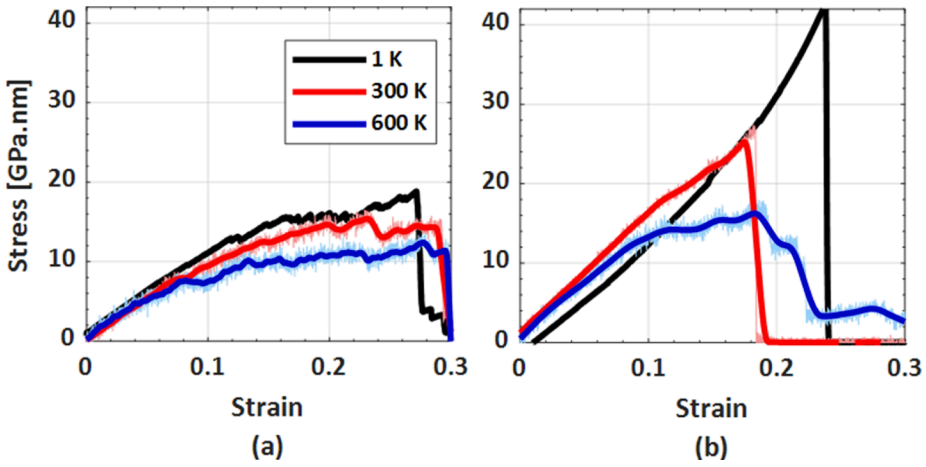

Fig. 16. Stress–strain curves of χ_3-BNT, (a) zigzag, (b) armchair.

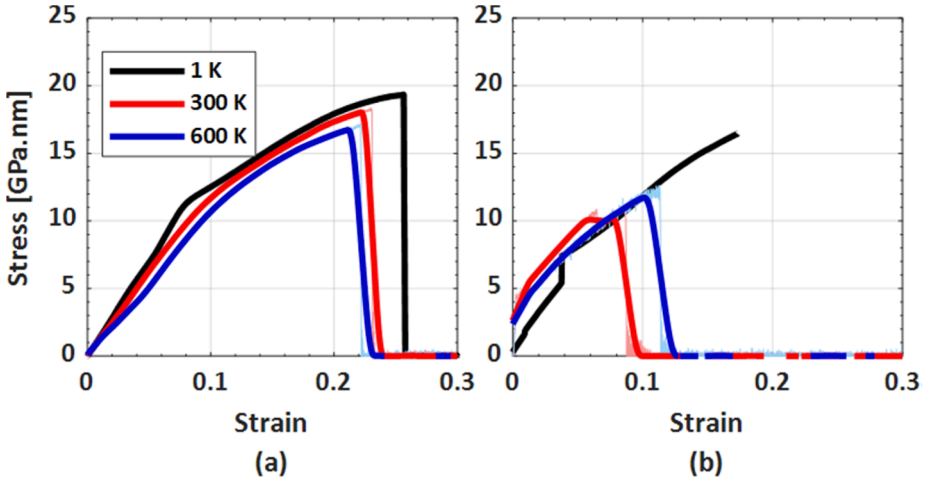

Fig. 17. Stress–strain curves of δ_3-BNT, (a) zigzag (b) armchair.

10^{10}, and 10^{11} 1/s. The stress-strain curves for those tensile loadings at varied rates are shown in Fig. S4. It can be observed that the loading rate effect on Young's moduli is much less significant compared to the effect on the ultimate tensile strength for all structures. In this regard, a distinguishable increase, especially for β_4 and β_{12}, in the tensile strengths are noticed as the loading rates increase. On the other hand, Young moduli of the structures 2-pmmn and χ_3 seem to be almost unaffected, while a slight increase is observed for β_4 and β_{12}.

4. Conclusion

This study demonstrates that reactive molecular dynamics can successfully represent unique aspects of the BNTs, including surface buckling and non-circular cross-section formations. Therefore, it can be concluded that ReaxFF potential can be safely utilized to investigate the mechanical properties. The tensile simulation results depict that the 2-pmmn zigzag BNT has the highest ultimate tensile strength and Young's modulus. In addition, χ_3 armchair, α armchair, and α zigzag structures have the highest ultimate tensile strength, strain, and Young's modulus, respectively, among the planar structures. Cross-sectional variations of the BNTs are noticed to be effective on the mechanical response of the BNTs. For instance, the β_{13}-BNT specimen is shown to degenerate to film-like planar structure within the deformation process due to bond formation between reciprocal atoms, which in turn results in hardening of the specimen. It is also observed that the ultimate tensile strength and stiffness of the structures generally decrease as the vacancy ratio or porosity and temperature increase. Furthermore, empirical formulae based on the vacancy ratio are developed to predict Young's moduli and ultimate tensile strength of BNTs with non-zero vacancy ratios. In conclusion, the results developed within this study indicate that thermally stable BNTs can be great analogs for other nanotubes such as CNTs and BNNTs with the advantage of their porous structure that can be exploited for several applications such as hydrogen storage.

CRediT authorship contribution statement

Erdem Caliskan: Visualization, Investigation, Validation, Methodology, Software, Data curation, Writing – original draft. **Mesut Kirca:** Conceptualization, Supervision, Writing – review & editing.

Declaration of Competing Interest

The authors declare that they have no known competing financial interests or personal relationships that could have appeared to influence the work reported in this paper.

Acknowledgements

Computing resources used in this work were partially provided by the National Center for High Performance Computing of Turkey (UHeM, grant numbers 1010562021 and 4010542021) and TUBITAK ULAKBIM, High Performance and Grid Computing Center (TRUBA).

Data availability

The raw/processed data required to reproduce these findings cannot be shared at this time as the data also forms part of an ongoing study.

Appendix A. Supplementary material

Supplementary data to this article can be found online at https://doi.org/10.1016/j.commatsci.2022.111368.

References

[1] S. Iijima, Helical microtubules of graphitic carbon, Nature 354 (6348) (1991) 56–58.
[2] A.K. Geim, K.S. Novoselov, The rise of graphene, Nat. Mater. 6 (2007) 183–191.
[3] B. Feng, J. Zhang, R.-Y. Liu, T. Iimori, C. Lian, H. Li, L. Chen, K. Wu, S. Meng, F. Komori, I. Matsuda, Direct evidence of metallic bands in a monolayer boron sheet, Phys. Rev. B 94 (4) (2016), 041408.
[4] P. Vogt, et al., Silicene: Compelling experimental evidence for graphenelike two-dimensional silicon, Phys. Rev. Lett. 108 (2012), 155501.
[5] B. Feng, et al., Evidence of silicene in honeycomb structures of silicon on Ag(111), Nano Lett. 12 (2012) 3507–3511.
[6] M.E. Dávila, L. Xian, S. Cahangirov, A. Rubio, G. Le Lay, Germanene: A novel two-dimensional germanium allotrope akin to graphene and silicene, New J. Phys. 16 (2014), 095002.
[7] L. Li, et al., Buckled germanene formation on Pt(111), Adv. Mater. 26 (2014) 4820–4824.
[8] A.J. Mannix, et al., Synthesis of borophenes: Anisotropic, two-dimensional boron polymorphs, Science (80-.) 350 (2015) 1513–1516.
[9] B. Feng, et al., Experimental realization of two-dimensional boron sheets, Nat. Chem. 8 (2016) 563–568.
[10] D.E. Sands, J.L. Hoard, Rhombohedral elemental boron, J. Am. Chem. Soc. 79 (20) (1957) 5582–5583.
[11] W.G. Woods, An introduction to boron: History, sources, uses, and chemistry, in: Environmental Health Perspectives, 102, Public Health Services, US Dept of Health and Human Services, 1994, pp. 5–11.
[12] T. Ogitsu, E. Schwegler, G. Galli, β-Rhombohedral Boron: At the Crossroads of the Chemistry of Boron and the Physics of Frustration, Chem. Rev. 113 (5) (2013) 3425–3449.
[13] J. Tian, Z. Xu, C. Shen, F. Liu, N. Xu, H.-J. Gao, One-dimensional boron nanostructures: Prediction, synthesis, characterizations, and applications, Nanoscale 2 (8) (2010) 1375.
[14] I. Boustani, A. Quandt, Nanotubules of bare boron clusters: Ab initio and density functional study, Europhys. Lett. 39 (1997) 527–532.
[15] D. Ciuparu, R.F. Klie, Y. Zhu, L. Pfefferle, Synthesis of Pure Boron Single-Wall Nanotubes, J. Phys. Chem. B 108 (2004) 3967–3969.
[16] F. Liu, et al., Metal-like single crystalline boron nanotubes: Synthesis and in situ study on electric transport and field emission properties, J. Mater. Chem. 20 (2010) 2197–2205.
[17] J. Liu, Z. Iqbal, Facile synthesis of pure boron nanotubes and nanofibers, Mater. Res. Soc. Symp. Proc. 1307 (2011) 42–47.
[18] J.W.G. Wilder, L.C. Venema, A.G. Rinzler, R.E. Smalley, C. Dekker, Electronic structure of atomically resolved carbon nanotubes, Nature 391 (6662) (1998) 59–62.
[19] T.W. Odom, J.-L. Huang, P. Kim, C.M. Lieber, Atomic structure and electronic properties of single-walled carbon nanotubes, Nature 391 (6662) (1998) 62–64.
[20] A. Sebetci, E. Mete, I. Boustani, Free standing double walled boron nanotubes, J. Phys. Chem. Solids 69 (8) (2008) 2004–2012.
[21] A.K. Singh, A. Sadrzadeh, B.I. Yakobson, Probing properties of boron a-tubes by Ab Initio calculations, Nano Lett. 8 (2008) 1314–1317.
[22] X. Yang, Y. Ding, J. Ni, Ab initio prediction of stable boron sheets and boron nanotubes: Structure, stability, and electronic properties, Phys. Rev. B – Condens. Matter Mater. Phys. 77 (2008), 041402.
[23] H. Tang, S. Ismail-Beigi, First-principles study of boron sheets and nanotubes, Phys. Rev. B – Condens. Matter Mater. Phys. 82 (2010) 1–20.
[24] N.G. Szwacki, C.J. Tymczak, The symmetry of the boron buckyball and a related boron nanotube, Chem. Phys. Lett. 494 (2010) 80–83.
[25] R.N. Gunasinghe, C.B. Kah, K.D. Quarles, X.Q. Wang, Dispersion corrections in the boron buckyball and nanotubes, Appl. Phys. Lett. 98 (2011), 261906.
[26] J. Kunstmann, V. Bezugly, H. Rabbel, M.H. Rümmeli, G. Cuniberti, Unveiling the atomic structure of single-wall boron nanotubes, Adv. Funct. Mater. 24 (2014) 4127–4134.
[27] V. Bezugly, J. Kunstmann, B. Grundkötter-Stock, T. Frauenheim, T. Niehaus, G. Cuniberti, Highly conductive boron nanotubes: Transport properties, work functions, and structural stabilities, ACS Nano 5 (6) (2011) 4997–5005.
[28] S. Wu, Z. Yang, A.-M. Guo, F. Ouyang, Electron transport along boron nanotubes rolled from β12-borophene: A first-principles study, Phys. E Low-Dimens. Syst. Nanostructures 126 (2021), 114457.
[29] Y. Ding, J. Ni, Electronic properties of boron nanotubes with axial strain, Front. Phys. China 4 (2009) 383–388.
[30] M.Q. Le, B. Mortazavi, T. Rabczuk, Mechanical properties of borophene films: A reactive molecular dynamics investigation, Nanotechnology 27 (44) (2016) 445709.
[31] H. Tang, S. Ismail-Beigi, Novel precursors for boron nanotubes: The competition of two-center and three-center bonding in boron sheets, Phys. Rev. Lett. 99 (2007), 115501.
[32] J. Kunstmann, A. Quandt, Constricted boron nanotubes, Chem. Phys. Lett. 402 (2005) 21–26.
[33] J. Kunstmann, A. Quandt, Broad boron sheets and boron nanotubes: An ab initio study of structural, electronic, and mechanical properties, Phys. Rev. B – Condens. Matter Mater. Phys. 74 (2006), 035413.
[34] M.H. Evans, J.D. Joannopoulos, S.T. Pantelides, Electronic and mechanical properties of planar and tubular boron structures, Phys. Rev. B – Condens. Matter Mater. Phys. 72 (4) (2005).
[35] A. Kochaev, Elastic properties of noncarbon nanotubes as compared to carbon nanotubes, Phys. Rev. B 96 (2017) 1–7.
[36] J. Zhang, J. Zhou, Buckling of boron nanotubes under axial compression: Insights from molecular mechanics and continuum mechanics, Phys. E Low-Dimens. Syst. Nanostruct. 127 (2021), 114520.
[37] B. Aziz, A.S. Asha, M.A. Ali, Evaluation of mechanical properties of borophene nanotube by molecular dynamics simulation, AIP Conf. Proc. 2324 (2021), 030022.
[38] Y.P. Zhou, J.W. Jiang, Molecular dynamics simulations for mechanical properties of borophene: Parameterization of valence force field model and Stillinger-Weber potential, Sci. Rep. 7 (2017) 1–12.
[39] B. Mortazavi, O. Rahaman, A. Dianat, T. Rabczuk, Mechanical responses of borophene sheets: A first-principles study, Phys. Chem. Chem. Phys. 18 (2016) 27405–27413.
[40] B. Mortazavi, M.Q. Le, T. Rabczuk, L.F.C. Pereira, Anomalous strain effect on the thermal conductivity of borophene: a reactive molecular dynamics study, Phys. E Low-Dimens. Syst. Nanostruct. 93 (2017) 202–207.
[41] S. Sadeghzadeh, Borophene sheets with in-plane chain-like boundaries; a reactive molecular dynamics study, Comput. Mater. Sci. 143 (2018) 1–14.
[42] S. Sadeghzadeh, M.M. Khatibi, Vibrational modes and frequencies of borophene in comparison with graphene nanosheets, Superlattices Microstruct. 117 (2018) 271–282.
[43] S. Arabha, A.H. Akbarzadeh, A. Rajabpour, Engineered porous borophene with tunable anisotropic properties, Compos. Part B Eng. 200 (2020), 108260.
[44] A. Stukowski, Visualization and analysis of atomistic simulation data with OVITO-the Open Visualization Tool, Model. Simul. Mater. Sci. Eng. 18 (2010) 015012.
[45] A.C.T. Van Duin, S. Dasgupta, F. Lorant, W.A. Goddard, ReaxFF: A reactive force field for hydrocarbons, J. Phys. Chem. A 105 (2001) 9396–9409.
[46] S.J. Pai, B.C. Yeo, S.S. Han, Development of the ReaxFFCBN reactive force field for the improved design of liquid CBN hydrogen storage materials, Phys. Chem. Chem. Phys. 18 (2016) 1818–1827.
[47] T.P. Senftle, et al., The ReaxFF reactive force-field: Development, applications and future directions, npj Comput. Mater. 2 (2016).
[48] K. Chenoweth, A.C.T. Van Duin, W.A. Goddard, ReaxFF reactive force field for molecular dynamics simulations of hydrocarbon oxidation, J. Phys. Chem. A 112 (2008) 1040–1053.
[49] H. Wang, et al., Strain effects on borophene: Ideal strength, negative Possion's ratio and phonon instability, New J. Phys. 18 (2016).
[50] X. Zhang, J. Hu, Y. Cheng, H.Y. Yang, Y. Yao, S.A. Yang, Borophene as an extremely high capacity electrode material for Li-ion and Na-ion batteries, Nanoscale 8 (33) (2016) 15340–15347.
[51] S. Plimpton, Fast parallel algorithms for short-range molecular dynamics, J. Comput. Phys. 117 (1) (1995) 1–19.
[52] H.M. Aktulga, J.C. Fogarty, S.A. Pandit, A.Y. Grama, Parallel reactive molecular dynamics: Numerical methods and algorithmic techniques, Parallel Comput. 38 (2012) 245–259.
[53] H.M. Aktulga, et al., Optimizing the performance of reactive molecular dynamics simulations for many-core architectures, Int. J. High Perform. Comput. Appl. 33 (2019) 304–321.
[54] R. Wu, et al., Large-area single-crystal sheets of borophene on Cu(111) surfaces, Nat. Nanotechnol. 14 (2019) 44–49.
[55] A. Mazaheri, M. Javadi, Y. Abdi, Chemical vapor deposition of two-dimensional boron sheets by thermal decomposition of diborane, ACS Appl. Mater. Interfaces 13 (2021) 8844–8850.
[56] S. Chahal, P. Ranjan, M. Motlag, S.S.R.K.C. Yamijala, D.J. Late, E.H.S. Sadki, G. J. Cheng, P. Kumar, Borophene via Micromechanical Exfoliation, Adv. Mater. 33 (34) (2021) 2102039.